Proc. Natl. Acad. Sci. USA
Vol. 96, pp. 3531–3536, March 1999
Biochemistry

Crystal structure of human type II inosine monophosphate dehydrogenase: Implications for ligand binding and drug design

THOMAS D. COLBY*, KRISTEN VANDERVEEN*, MICHAEL D. STRICKLER*, GEORGE D. MARKHAM†, AND BARRY M. GOLDSTEIN*‡

*Department of Biochemistry and Biophysics, University of Rochester Medical Center, 601 Elmwood Avenue, Rochester, NY 14642, and †Institute for Cancer Research, Fox Chase Cancer Center, Philadelphia, PA 19111

Communicated by Judith P. Klinman, University of California, Berkeley, CA, January 25, 1999 (received for review October 5, 1998)

ABSTRACT **Inosine monophosphate dehydrogenase (IMPDH) controls a key metabolic step in the regulation of cell growth and differentiation. This step is the NAD-dependent oxidation of inosine 5′ monophosphate (IMP) to xanthosine 5′ monophosphate, the rate-limiting step in the synthesis of the guanine nucleotides. Two isoforms of IMPDH have been identified, one of which (type II) is significantly up- regulated in neoplastic and differentiating cells. As such, it has been identified as a major target in antitumor and immunosuppressive drug design. We present here the 2.9-Å structure of a ternary complex of the human type II isoform of IMPDH. The complex contains the substrate analogue 6-chloropurine riboside 5′-monophosphate (6-Cl-IMP) and the NAD analogue selenazole-4-carboxamide adenine dinucleotide, the selenium derivative of the active metabolite of the antitumor drug tiazofurin. The enzyme forms a homotetramer, with the dinucleotide binding at the monomer–monomer interface. The 6 chloro-substituted purine base is dehalogenated, forming a covalent adduct at C6 with Cys-331. The dinucleotide selenazole base is stacked against the 6-Cl-IMP purine ring in an orientation consistent with the B-side stereochemistry of hydride transfer seen with NAD. The adenosine end of the ligand interacts with residues not conserved between the type I and type II isoforms, suggesting strategies for the design of isoform-specific agents.**

The control of cell growth and differentiation is fundamental to a wide variety of biological functions. Chemotherapeutic intervention in pathological differentiation and growth (antitumor therapy) or in normal cellular responses to external antigens (immune suppression) is greatly enhanced by the identification of an enzymatic target and the design of agents to interact with this target in a specific manner. Inosine monophosphate dehydrogenase (IMPDH, EC 1.1.1.205) has been identified as a key enzyme in the regulation of cell proliferation and differentiation (1–3). An extensive literature now addresses the characterization, mechanism, and biological functions of IMPDH, its role as a target for both antileukemic and immunosuppressive therapy, and its inhibition by chemotherapeutic agents (for reviews, see refs. 1–3).

IMPDH catalyzes the rate-limiting step in the *de novo* synthesis of the guanine nucleotides, the nicotinamide adenine dinucleotide (NAD)-dependent oxidation of inosine 5′-monophosphate (IMP) to xanthosine 5′ monophosphate (XMP) (4, 5). After substrate addition, nucleophilic attack of an active site cysteine (Cys-331) on the IMP base forms a covalent intermediate. Binding of cofactor NAD results in hydride transfer to the B-side of the nicotinamide ring to form product XMP (6–10).

Given the central position of IMPDH in guanine nucleotide synthesis, inhibition of the enzyme results in a number of chemotherapeutically useful sequelae. Inhibition of IMPDH produces an overall reduction in guanine nucleotide pools. Subsequent interruption of DNA and RNA synthesis results in cytotoxicity (11). The reduction in guanine nucleotides also compromises the ability of G proteins to function as transducers of intracellular signals (12–16). IMPDH inhibition results in down-regulation of c-*myc* and/or Ki-*ras* oncogenes in a number of human tumor cell lines (1, 13, 17, 18). Signaling effects are accompanied by induction of cell differentiation and apoptosis (1, 2, 17–19).

The effects of IMPDH inhibition have been widely investigated and exploited in antitumor chemotherapy by using the C-nucleoside analogue tiazofurin (1). *In vivo*, tiazofurin is converted into the NAD analogue thiazole-4-carboxamide adenine dinucleotide (TAD), in which the nicotinamide ring is replaced by the thiazole-4-carboxamide moiety (20). TAD is a noncompetitive inhibitor of IMPDH with respect to NAD, with a K_i of $\approx$0.2 μM (20). Kinetic studies suggest that TAD inhibits IMPDH by binding at the NAD site (6).

Tiazofurin has demonstrated significant antitumor activity in a wide variety of tumor systems (17, 18, 21–24). In recent phase II trials, tiazofurin induced complete hematologic remissions in patients with end-stage acute nonlymphocytic leukemia or in myeloblastic crisis of chronic myeloid leukemia (25, 26). The efficacy of tiazofurin is associated with its dual antiproliferative and myeloid differentiation-inducing activities (1, 25–27). Both effects are attributed to a reduction in intracellular guanine nucleotide pools due to inhibition of IMPDH by the dinucleotide analogue TAD (1, 26).

Inhibition of IMPDH is also used as a strategy in immunosuppressive therapy. Growth and differentiation of human lymphocytes are particularly dependent on the IMPDH-catalyzed *de novo* pathway for purine nucleotide synthesis (28). Inhibition of IMPDH leads to suppression of both T and B lymphocyte proliferation (2). Mycophenolate mofetil, the prodrug of the IMPDH inhibitor mycophenolic acid (MPA), is approved as an immunosuppressant in the treatment of acute rejection in renal transplants (29, 30). MPA is a substituted benzolactone that acts as an uncompetitive inhibitor of IMPDH with K_is in the range 0.01–0.03 μM (31). Like TAD, MPA binds IMPDH at the putative NAD site (6, 32).

Despite the availability of IMPDH inhibitors, lack of specificity remains a problem in their clinical use (33). Efficacy achieved in phase II trials of tiazoforin required hospitalization and aggressive treatment of neuro- and cardiovascular toxicities (25, 26). Although less severe, the gastrointestinal toxicity of MPA, coupled with its rapid metabolism to the biologically inactive glucoronide, remain dose limiting as well (29, 30). Whereas the role of

The publication costs of this article were defrayed in part by page charge payment. This article must therefore be hereby marked "*advertisement*" in accordance with 18 U.S.C. §1734 solely to indicate this fact.

PNAS is available online at www.pnas.org.

Abbreviations: 6-Cl-IMP, 6-chloropurine riboside 5′-monophosphate; IMP, inosine 5′-monophosphate; IMPDH, inosine 5′-monophosphate dehydrogenase; MPA, mycophenolic acid; SAD, selenazole-4-carboxamide adenine dinucleotide; TAD, thiazole-4-carboxamide adenine dinucleotide; XMP, xanthosine 5′-monophosphate.

Data deposition: The atomic coordinates have been deposited in the Protein Data Bank, Biology Department, Brookhaven National Laboratory, Upton, NY 11973 (PDB ID code 1b3o).

‡To whom reprint requests should be addressed.

MPA as an antitumor agent has not been vigorously investigated, early clinical trials showed the agent to be ineffective in chemotherapy (34, 35). More recent *in vivo* studies suggest that the antitumor efficacy of MPA is also limited by rapid metabolic inactivation (36, 37). In both antitumor and immunosuppressive therapy, improvement in inhibitor specificity may reduce toxicity and enhance efficacy.

A strategy for providing more directed IMPDH therapy is suggested by the discovery of two isoforms of the enzyme, labeled type I and type II (38). These are of identical size and share 84% sequence identity, but appear to serve different roles. The type I isoform is constitutively expressed and is the major species found in normal lymphocytes (39–42). However, the expression of type II IMPDH is up-regulated in human leukemic cell lines (39), human ovarian tumors (38), and leukemic cells from patients with chronic granulocytic, lymphocytic, and acute myeloid leukemias (41). This results in an 8- to 9-fold increase in activity of type II vs. type I IMPDH in *in vitro* leukemic lines (39). Conversely, Type II expression is down-regulated over 90% in either HL-60 cells induced to differentiate (42) or in patient leukemic cells treated *in vitro* (41).

Thus, type II IMPDH is an inducible enzyme whose role is closely linked to cell differentiation and neoplastic transformation (2). The disproportionate increases in IMPDH activity in malignant cells has made this enzyme a key target for specific antileukemic chemotherapy (1). Although normal human T lymphocytes appear to induce both type I and type II enzymes when stimulated by mitogen (43), isozyme specificity remains a goal for immunosuppressive therapy as well (31).

The design of isoform-specific agents will be aided by identification of enzyme–ligand interactions both common and unique to each isoform. Recently, a 2.6-Å crystal structure of hamster IMPDH was obtained (32). The hamster enzyme is highly homologous to the human type II isoform and was crystallized as a complex containing substrate IMP and inhibitor MPA. Because MPA binds in the putative nicotinamide pocket, the structure does not contain NAD (6, 32). In addition, all residues identified as directly interacting with MPA are conserved between IMPDH type I and type II in the human enzyme. This precludes identification of any obvious exploitable differences in the design of agents specific for one isoform over the other. A second structure of IMPDH from the protozoan *Tritrichomonas foetus* has also appeared (44). This structure shares 25–30% sequence identity with known mammalian forms of the enzyme. This complex contains product XMP but no inhibitor or cofactor (44).

Although these structures provide a great deal of information about substrate binding and enzyme mechanism, information relevant to dinucleotide inhibitor design is missing. This includes definition of the NAD site, the interactions characterizing the binding of cofactor or dinucleotide analogues, and conformational changes associated with cofactor binding. Thus, we have undertaken the structure determination of a ternary complex of human type II IMPDH. This complex contains the halogenated substrate analogue 6-Cl IMP and the NAD analogue selenazole-4-carboxamide adenine dinucleotide (SAD), the active selenium analogue of the tiazofurin metabolite TAD (45, 46). We identify unique structural features relevant to IMPDH-cofactor binding, as well as potentially exploitable differences between the type I and type II isoforms.

EXPERIMENTAL PROCEDURES

Expression and Purification of Human Type II IMPDH. Human type II IMPDH was expressed in *Escherichia coli* strain BL21(DE3)pIMP as described in ref. 47. Expressed IMPDH was purified from the supernatant using ion exchange chromatography. Centrifuged lysate was loaded onto a PerSeptive Biosystems (Framingham, MA) HS cation exchange column (1.6 ml volume) equilibrated in a cation buffer containing 6.7 mM each of Hepes, Mes, and Na acetate buffers at pH 7.2. IMPDH was eluted with a linear 0–1,000 mM NaCl gradient over 6 column volumes using the BioCad Sprint perfusion chromatography system. Fractions with high IMPDH activity were pooled and loaded onto a Q-Sepharose (Amersham Pharmacia) anion exchange column (2.5 × 10 cm) equilibrated in Buffer A (50 mM Tris·HCL/50 mM KCl/2 mM EDTA/2 mM DTT, pH 8.0 at 4°C). Enzyme was eluted by using a linear gradient of 50–1,000 mM KCl over three column volumes by using the Gradifrac system (Amersham Pharmacia). Fractions with high IMPDH activity were pooled and desalted using Centriprep-10 concentrators (Amicon). IMPDH activity was monitored by XMP production at 290 nm (ε_{290} = 4600 M^{-1} cm^{-1}) in 50 mM Tris·HCL/10 mM KCl/1 mM DTT, pH 8.00 (20°C) with 0.2 mM IMP. The reaction was initiated by addition of 0.2 mM NAD. Purity of the human type II IMPDH was estimated to be >99% by silver-stained SDS/PAGE.

Crystallization of Type II IMPDH-6-Cl-IMP-SAD Complex. Pure apo-IMPDH (1 mg/ml) was inhibited by a 30-min room-temperature incubation with a 10-fold molar excess of 6-chloropurine riboside 5′monophosphate (6-Cl-IMP) (Sigma). The complex was concentrated and exchanged into fresh Buffer A (above). Crystals were grown by using vapor diffusion techniques: 2 μl protein (5 mg/ml in Buffer A) was mixed with 2 μl reservoir solution [4–6% polyethylene glycol 6000/1 M LiCl/100 mM Tris, pH 8.0 or 8.2/5% methylpyrollidinone (vol/vol)/24 mM β-mercaptoethanol], and equilibrated over the reservoir solution at 4°C. Resulting tetrahedral crystals were used to seed 4 μl drops of identical composition, yielding diffraction-quality crystals within 48 hr. The dinucleotide inhibitor SAD was introduced by adding ≈40 μg solid inhibitor to the 4-μl droplet containing the crystals. SAD was obtained from K. Pankiewicz and K. Watanabe, prepared according to the methods of Marquez (45).

X-Ray Data Collection. Small (≈0.15 mm) colorless tetrahedral crystals were soaked ≈30 sec in 10-μl drops of mother liquor containing successively 10%, 20%, and 30% polyethylene glycol 400. Crystals were loop mounted and flash frozen at −180°C by using standard cryocrystallization methods (48). Initial characterization was performed in house. Data were obtained from a single crystal on the CCD detector at the Cornell High Energy Synchrotron Source A1 beam line. Data were processed and reduced by using local software and DENZO and SCALEPACK (49). The crystal showed diffraction to a minimum *d*-spacing of 2.8 Å, but only data to 2.9 Å were used. Data collection and reduction statistics are summarized in Table 1.

Structure Solution and Refinement. Crystals were not isomorphous to either the hamster or *T. foetus* forms. The α/β core domain of the hamster enzyme was used as a search model in a molecular replacement solution (50). The hamster monomer was truncated, leaving a search model containing 298 of the 514 residues. The self-rotation search indicated a noncrystallographic 2-fold axis in the *xy* plane normal to the crystallographic tetramer 4-fold axis. Crossrotation searches with the truncated hamster model, followed by Patterson correlation refinement using X-PLOR 3.853 (51) indicated the presence of two monomers in the asymmetric unit related by the noncrystallographic 2-fold axis. Translation searches performed on the PC-refined rotation solutions provided the positions of the independent monomers, defining an octamer consisting of two closely packed tetramers related by the noncrystallographic 2-fold.

This model was subjected to conjugate-gradient refinement with NCS restraints in CNS (52) using a maximum likelihood target function based on intensities (53). Subsequent σ_A-weighted maps (54) revealed density with approximate 2-fold symmetry corresponding to the majority of the flanking domain of one monomer. Manual model building followed by real-space and positional refinement in CNS permitted fitting of 90 of the 120 residues in this domain.

The resulting crystal packing indicated only edge-on contacts between octamers, with a large 75 × 100-Å "hole" between octamers along the *z* axis. A similar 85-Å solvent-filled cavity is observed in the *T. foetus* structure (44). The larger cavity ob-

Table 1. Data collection and refinement statistics

Measurement	Value
X-ray source	CHESS beamline A-1
Wavelength, Å	0.91
Detector	CCD
Temperature, °C	−180
d_{min}, Å	2.9
Space group	I4
Unit cell, Å a,b	142.3
c	174.9
Total number of observations	126775
Unique reflections ($I/\sigma > 0$)	34001
Completeness (overall), %	86.4
(3.0-2.9 Å shell),%	56.2
R_{sym} (overall), %	9.5
(3.0-2.9 Å shell)%	33.8
I/σ (overall)	10
(3.0-2.9 Å shell)	3
Monomers in asymetric unit	2
Non-H atoms in asymetric unit	5521
R_{cryst}, %	24.4
R_{free}, %	27.0
rms, bonds, Å	0.012
angles, deg.	1.9
dihedrals, deg.	23.1
impropers, deg.	1.05
Ordered solvent molecules	31

$R_{sym} = \Sigma|I - \langle I\rangle|/\Sigma I$, where I is an individual reflection measurement and $\langle I\rangle$ is the mean intensity for symmetry-related reflections.

$R_{cryst} = \Sigma\|F_o| - |F_c\|/\Sigma|F_o|$ where F_o and F_c are observed and calculated structure factors, respectively.

R_{free} is calculated by using a randomly selected subset comprising 10% of reflections that were excluded from all stages of refinement.

served here yields an unusually high Matthews' coefficient of ≈3.9 Å^3/dalton (50). This volume is sufficient to accommodate a single tetramer stacked along z. However, a variety of density modification techniques using DM (55) failed to yield any features in this region, and systematic translation searches along z yielded no additional peaks. Exhaustive direct-space searches using a variety of disordered models also failed to produce any improvement in crystallographic residuals. These findings indicated that, if present, the additional tetramer is highly disordered.

Simulated annealing (SA) of the two-monomer model followed by calculation of σ_A-weighted SA-omit maps (56) of the active site yielded density corresponding to the bound ligands. Subsequent cycles of model building and annealing were performed to obtain models for the ligands and to refit the active site loop (residues 325–342) adjacent to the substrate analogue. Constraints were placed on ligand ring planarity and sugar puckers and on the geometry of the covalent connection between the IMP analogue and the active site loop. A final stage of conjugate gradient refinement with NCS restraints on α-carbon positions was followed by individual B-factor refinement. Despite reasonable density (Fig. 3), high B-factors for the selenazole end of the dinucleotide led to a lowering of its occupancy to 0.75. At this occupancy, thermal factors of the ligand adenosine ring more closely match those of adjacent residues.

As observed in previous structures, the human enzyme displays significant regions of disorder. Nevertheless, 410 of 514 residues and both ligands have been refined in the more complete of the two independent monomers. This is comparable to final models obtained for the hamster and *T. foetus* structures (405 of 514 and 332 of 503 residues, respectively). In the final model, two non-glycine residues (Ala-338 and Thr-116) fall just outside of allowed regions of the Ramachandran plot. These are located in highly flexible regions of the structure. Final refinement statistics are provided in Table 1.

RESULTS

General Features. The complex of the human enzyme demonstrates the same tetrameric organization observed in the hamster and *T. foetus* structures (32, 44) (Fig. 1). The sequence of human IMPDH type II differs from that of the hamster enzyme by only six amino acids (32). Thus, major differences in tertiary structure between the human and hamster enzymes were not expected. Each monomer consists of two domains: a major catalytic domain and a smaller flanking domain (Fig. 1). Whereas the overall folds of these domains are similar to those reported for the hamster enzyme (32), differences are observed.

The 394-residue catalytic domain forms an eight-stranded parallel α/β barrel core with attached N- and C-terminal sections. The active site is bounded by one face of the barrel, as well as an 18-residue "loop" (residues 325–342) and 54-residue "flap" (residues 398–451) inserted on the barrel face. The active site loop and flap regions show significant conformational changes relative to previous structures (32). These are described below.

The 120-residue flanking domain (residues 113–232) lies adjacent to the catalytic domain, inserted between the α2 helix and β3 sheet of the barrel (Fig. 1). The function of the flanking domain in IMPDH is unknown, and it is apparently not required for activity (32). A search of the flanking domain sequence in the ProDom domain database (57) identified two copies of a cystathionine β-synthase-like domain (58) as the closest homologue. This is consistent with the observation of approximate 2-fold symmetry in the β-sheet region of this domain in the human structure.

The relative positions of the catalytic and flanking domains differ between the human and hamster enzymes, likely as a result of the different crystal packing observed between the structures. The angle between the catalytic and flanking domains is markedly more acute than that found in the hamster enzyme (32) (Fig. 2*A*), resulting from an ≈120° rotation about a vector normal to the two covalent linkages between the domains. This identifies a highly flexible hinge region at residues 111–113 and 225–227.

Dinucleotide Ligand Binding. σ_A-Weighted omit maps (56) in the SAD-soaked complex clearly indicate interpretable density

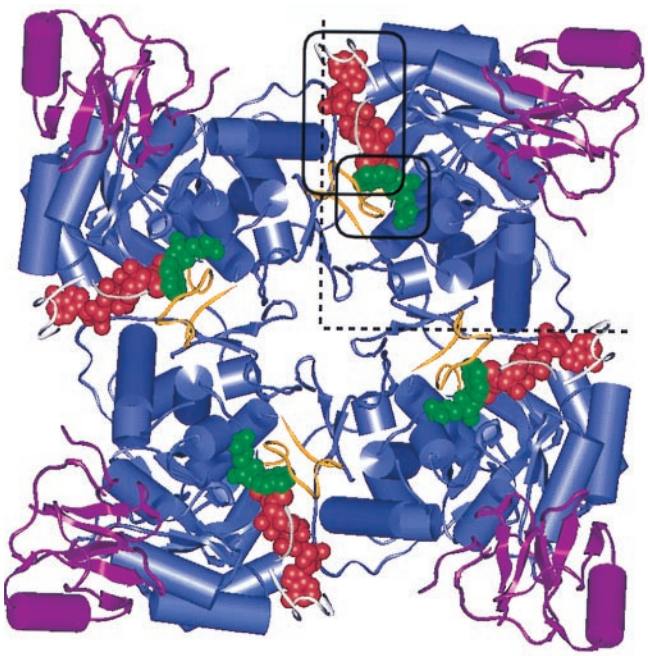

FIG. 1. Human Type II IMPDH tetramer with bound dinucleotide analogue SAD (circled, red) and substrate analogue 6-Cl-IMP (circled, green). The dinucleotide binds at the monomer–monomer interface (dotted lines). The following structures are illustrated: catalytic β-barrel domain (blue), flanking domain (magenta), active site loop (yellow) and active site flap fragments (white).

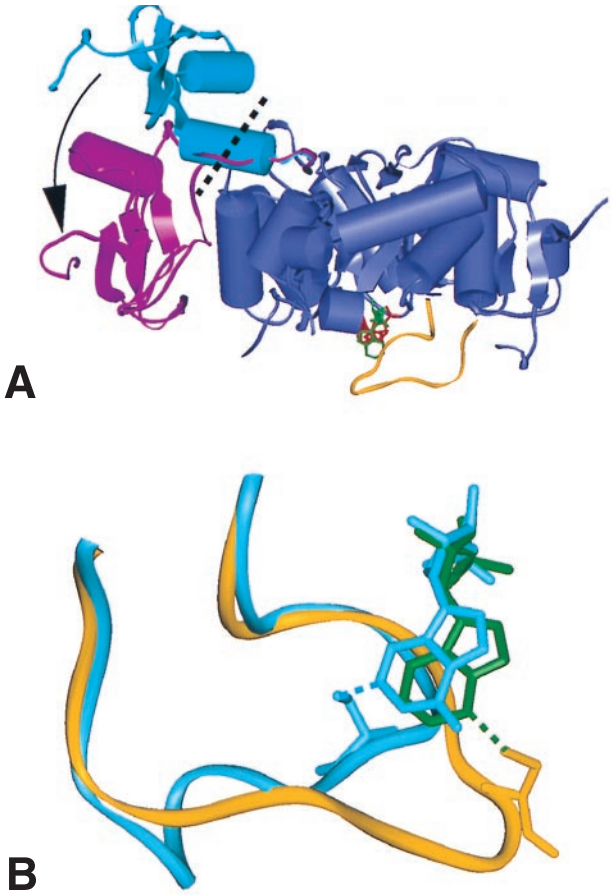

FIG. 2. (*A*) Comparison of flanking domain positions in the human (magenta) and hamster (cyan) (32) complexes. The two conformations are related by a rotation (arrow) about a vector through the hinge region (dotted black line). Flanking domains are 75% and 44% complete in the human and hamster models, respectively. Also shown are the core domain (blue), active site loop (yellow), and ligands (red and green). (*B*) Comparison of the active site loop observed in the human (yellow) and hamster (cyan) complexes. Purine rings for IMP (cyan) and 6-Cl-IMP (green) are shown. The IMP C2-Cys-331 adduct (cyan dotted line) seen in the hamster complex (32) is replaced by a C6-Cys-331 adduct here (green dotted line). This displaces the loop (yellow) to the opposite side of the purine ring.

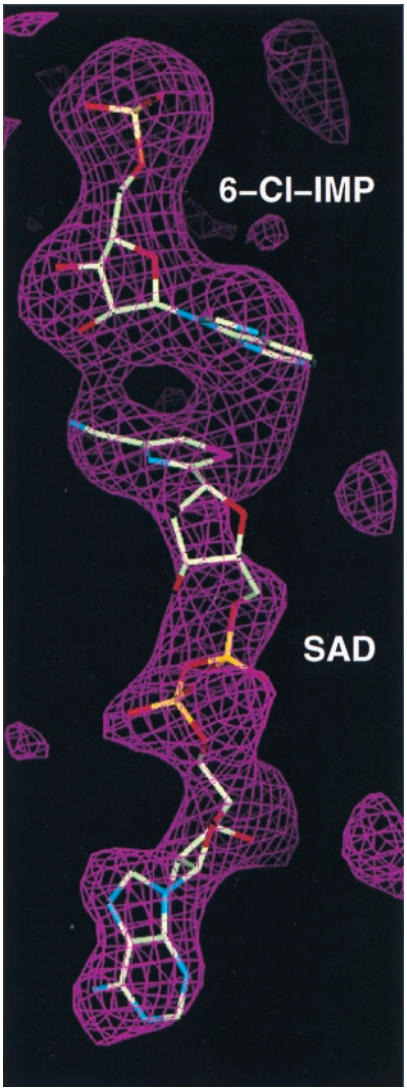

FIG. 3. σ_A-weighted Fo-Fc omit map illustrating SAD and 6-Cl-IMP binding. The dinucleotide selenazole ring stacks in the *anti* position against the 6-Cl-IMP purine ring. Analogous binding of cofactor NAD would favorably position the nicotinamide ring for B-side specific hydride transfer. The map was computed at the 2-σ level with both ligands omitted. Bond colors are: Se, magenta; P, yellow; O, red; N, blue; C, white.

corresponding to bound substrate analogue 6-Cl-IMP and bound dinucleotide analogue SAD (Fig. 3). Fitting of ligands into the observed density yields interesting findings. Chief among these is that the dinucleotide analogue SAD binds in a pocket extending from the active site to the monomer–monomer interface (Fig. 1). Further, several residues that closely interact with the ligand are not conserved between the type I and type II isoforms, providing potentially exploitable differences for drug design.

The SAD selenazole ring stacks against the 6-Cl-IMP base in the putative nicotinamide binding pocket of the active site (Fig. 3). Similar stacking is also observed between substrate and MPA in the hamster complex (32). Continuous density between the SAD carboxamide group and the O2′ hydroxyl of 6-Cl-IMP suggests a stabilizing hydrogen bond between inhibitor and substrate analogue (Fig. 3). A second interaction is observed between the carboxamide group and conserved residue Asn-303. These interactions are consistent with the requirement of a carboxamide group in the 4 position of the thiazole or selenazole heterocycle for activity (11, 59).

Poor density and high thermal parameters for the selenazole ribose indicate some disorder in this region of the ligand. However, best fits to density suggest that both intra- and intermolecular selenium–nucleophile contacts observed previously are maintained in IMPDH-bound SAD. The selenazole ring appears to bind in the *anti* conformation, with the Se atom adjacent to the furanose oxygen (Fig. 3). This preserves an intramolecular Se–O interaction observed in nucleoside structures (60) and in the alcohol dehydrogenase-bound β-methylene analogue of SAD (61). In addition, the electrophilic selenium forms a close intermolecular contact with the ε oxygen of Gln-334. An analogous intermolecular sulfur–oxygen interaction is seen in the β-methylene analogue of TAD bound to *Pseudomonas* exotoxin A (62).

The adenosine end of the dinucleotide analogue is bound in a cleft between the α3 helix–β3 sheet junction of one monomer and the βC–βD sheet junction of the adjacent monomer. A number of specific intermonomer protein–ligand interactions can be clearly identified. The dinucleotide adenine ring is stacked between the side chains of Phe-282 and His-253 near the α3 helix (Fig. 4). In this position, it makes two edge-on contacts. Density is observed between the adenine amino group and the side chain of residue Thr-252. On the opposite side of the ring, a contact is observed between adenine N3 and the side chain of Thr-45 on the adjacent monomer (Fig. 4). Two additional residues from the neighboring monomer interact with the adenine ribose. Gln-469 forms hydrogen bonds with both hydroxyl oxygens (Fig. 4), and

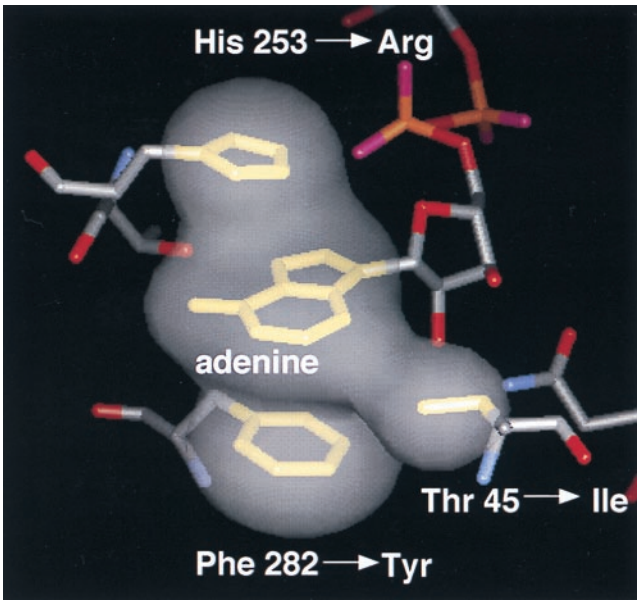

FIG. 4. Environment of the dinucleotide analogue adenine ring. Interacting residues are highlighted in yellow and outlined by van der Waals surfaces. In the human type II complex, the adenine ring is tightly stacked between Phe-282 and His-253, and makes close edge-on contacts with Thr-45 (*Right*) and Thr-252 (*Left*, not labeled). In the human type I isoform, residues 45, 253 and 282 are substituted as indicated. Thr-45 and adjacent Gln-469 (right, not labeled) are contributed by the neighboring monomer.

the main chain nitrogen of Ala-46 forms a water-mediated H-bond with O3′. Other polar contacts are observed between adenine and selenazole phosphate oxygens and adjacent serines 275 and 276, respectively.

Potentially exploitable differences between the type I and type II isoforms are observed in residues interacting with the dinucleotide. Among the residues interacting with the adenosine diphosphate component of the ligand, Thr-252, Gln-469, and the two serines 275 and 276 are either strictly or functionally conserved in eukaryotic IMPDH sequences. However, three of the four residues interacting with the adenosine ring in human type II IMPDH are *not* conserved between the human type I and type II isoforms (38). Thr-45 and the two adenosine-stacking residues Phe-282 and His-253 are replaced by Ile-45, Tyr-282, and Arg-253 in the type I isoform (38) (Fig. 4).

Dinucleotide Binding and the Active-Site Flap. A pair of β-strands comprising residues 400–450 has been previously identified as forming an active site flap that potentially stabilizes binding of substrate (32). In this complex, the majority of the flap residues are disordered. A limited but significant exception is observed adjacent to the adenine end of the dinucleotide. Here, a region of continuous well ordered density allows fitting of backbone fragments comprising a 10-residue turn and a 5-residue section of β-sheet (Fig. 1). Although side chain density is observed in this region, unambiguous residue assignments cannot be made at this resolution, nor can the fragments be unambiguously traced back to the main chain. Thus, these residues are not included in the final model. However, the position of these fragments relative to that of the proximal sections of flap identified in the hamster complex (32) suggests that this density may represent the terminal portion of the active site flap. This region is apparently disordered in the absence of a dinucleotide ligand (32, 44).

The putative sections of active site flap observed here contact the adenosine end of the dinucleotide (Fig. 1) both directly and by means of intervening residues. These contacts would continue the series of interactions with IMP formed by the proximal part of the flap seen in the hamster complex and suggest that the entire flap serves to stabilizes both substrate and dinucleotide binding.

6-Cl-IMP and the Active-Site Loop. 6-Cl-IMP is the halogenated analogue of the substrate IMP. Labeling studies have demonstrated that 6-Cl IMP inactivates IMPDH by undergoing NAD-independent dehalogenation, accompanied by covalent modification of active site residue Cys-331 (10). In the present complex, continuous density is observed between the 6-position on the inosine ring and the side chain of Cys-331, implying formation of a covalent adduct between the Cys-331 thiol and the dehalogenated C6 carbon on the ligand base.

Cys-331 also forms a covalent thio adduct with the normal substrate IMP as part of the catalytic mechanism (63, 64). This adduct is formed by sulfhydryl attack on C2 of the inosine ring and is observed in the crystal structure of the hamster IMPDH—MPA–IMP complex (32).

6-Cl-IMP binds in the same site occupied by IMP in the hamster enzyme (Fig. 2*B*). The conformation of the dehalogenated substrate analogue observed here is very similar to that of IMP (32). In particular, the orientation of the base relative to the ribose is *anti* in both complexes (Fig. 2*B*). Thus, formation of the C6-Cys-331 adduct observed here requires that Cys-331 be positioned on the opposite side of the inosine base from that required to form the C2 adduct seen in the hamster complex. This is accomplished by shifting the loop containing residues 325–340 to the C6 side of the substrate base (Fig. 2*B*). The additional length required for this movement is obtained by unwinding of the short αD helix observed in the hamster structure.

The alternative binding of the loop places it in the region occupied by the beginning of the active site flap in the hamster enzyme. In the hamster complex, this section of the active site flap forms one side of the IMP binding site, with residues 411, 414, 415, and 441 directly interacting with the IMP hypoxanthine ring and phosphate moiety (above) (32). These flap residues are disordered here, possibly as a result of displacement by the reoriented loop. The opposite surface of the IMP binding site remains unaffected by displacement of the loop. Thus, other enzyme–ligand polar interactions identified previously are preserved. These include H-bonds between the ribose hydroxyls and Ser-68 and Asp-364 and between the 5′-phosphate oxygens and residues 329, 366, 387, and 388.

SUMMARY AND DISCUSSION

The structure of a ternary complex between the human type II isoform of IMPDH and the substrate and cofactor analogues 6-Cl IMP and SAD provides insight into the mechanism of cofactor binding and the design of type-II specific agents.

Binding of the selenazole-4-carboxamide group observed here may mimic that of the NAD nicotinamide group. The selenazole-4-carboxamide group occupies the site identified as the putative nicotinamide binding pocket (6, 32). Stacking of the NAD nicotinamide ring against the IMP base in the same orientation as that observed for the SAD selenazole moiety would favorably position the nicotinamide ring for hydride transfer (Fig. 3). In this orientation, the nicotinamide ring would lie in the *anti* conformation relative to the ribose sugar, consistent with NMR studies suggesting that this conformation is adopted by IMPDH-bound NAD (65). Further, hydride transfer would occur to the B-side of the nicotinamide ring, consistent with the fact that IMPDH is a B-side specific enzyme (2).

Enzyme–ligand interactions in the 6-Cl-IMP complex likely suffer some distortion relative to those expected in the presence of normal substrate and cofactor. The use of this substrate analogue results in a thio-linkage between Cys-331 and the dehalogenated 6-position of the purine ring. This C6 adduct is obtained by shifting the active site loop from the location observed in complexes with IMP (32) (Fig. 2*B*). The reconfigured loop in turn displaces the near portion of the active site flap, disrupting interactions observed previously between flap and

IMP (32), and likely disrupting interactions with the dinucleotide ribose as well.

Nevertheless, a number of additional enzyme–IMP interactions observed previously are preserved here. Further, the presence of the SAD dinucleotide analogue may partially order the end of the active site flap, suggesting that the flap may stabilize both substrate and cofactor binding in the normal ternary complex. This is consistent with the observation that substrate-induced protection of the flap against proteolysis is enhanced by cofactor binding (66).

Protein–ligand interactions at the adenine end of SAD are well defined and are likely to be preserved in NAD binding as well. These include interactions with residues from adjacent monomers in the tetrameric complex, supporting the requirement of a tetrameric structure for activity (31). These interactions include two direct hydrogen bonds between the ribose hydoxyls and Gln-469, a water-mediated H-bond between the O3′ hydroxyl and the main chain of residue 46, and an edge-on contact between the adenine base and Thr-45. Dinucleotide-mediated interactions across monomer boundaries are unusual. Among 87 NAD complexes in the Protein Data Bank representing 29 different NAD-dependent enzymes, only glyceraldehyde-3-phosphate dehydrogenase-bound NAD forms hydrogen bonds with residues on an adjacent monomer.

The adenosine–protein interactions observed in the human type II IMPDH complex may also have application in the design of isoform-specific agents. Significant among these is an adenine "sandwich" formed by stacking of the ligand base between His-253 and Phe-282 (Fig. 4). Each of the residues previously identified as directly interacting with MPA is conserved between the type I and type II isoforms (32, 38). In contrast, three of the four residues making contact with the adenine ring of SAD are not conserved between isoforms (Fig. 4), offering potentially exploitable differences for the design of agents with greater specificity for the type II enzyme. Active and effective IMPDH inhibitors have recently been designed that incorporate an adenosine monophosphate moiety covalently linked to MPA (67). Such agents will prove particularly useful in exploiting the isoform-dependent differences in adenine binding identified here.

The authors are indebted to Drs. Krzysztof W. Pankiewicz and Kyoichi A. Watanabe, Pharmasset, Inc., for the SAD ligand.

1. Weber, G., Prajda, N., Abonyi, M., Look, K. Y. & Tricot, G. (1996) *Anticancer Res.* **16,** 3313–3322.
2. Wu, J. C. (1994) *Perspect. Drug Discovery Des.* **2,** 185–204.
3. Franklin, T. J., Edwards, G. & Hedge, P. (1994) *Adv. Exp. Med. Biol.* **370,** 155–160.
4. Weber, G., Prajda, N. & Jackson, R. C. (1976) *Adv. Enzyme Regul.* **14,** 3–24.
5. Jackson, R. C., Weber, G. & Morris, H. P. (1975) *Nature (London)* **256,** 331–333.
6. Hedstrom, L. & Wang, C. C. (1990) *Biochemistry* **29,** 849–854.
7. Wang, W. & Hedstrom, L. (1997) *Biochemistry* **36,** 8479–8483.
8. Xiang, B. & Markham, G. D. (1997) *Arch. Biochem. Biophys.* **348,** 378–382.
9. Antonino, L. C. & Wu, J. C. (1994) *Biochemistry* **33,** 1753–1759.
10. Antonino, L. C., Straub, K. & Wu, J. C. (1994) *Biochemistry* **33,** 1760–1765.
11. Jayaram, H. N., Dion, R. L., Glazer, R. I., Johns, D. G., Robins, R. K., Srivastava, P. C. & Cooney, D. A. (1982) *Biochem. Pharmacol.* **31,** 2371–2380.
12. Manzoli, L., Billi, A. M., Gilmour, R. S., Martelli, A. M., Matteucci, A., Rubbini, S., Weber, G. & Cocco, L. (1995) *Cancer Res.* **55,** 2978–2980.
13. Mandanas, R. A., Leibowitz, D. S., Gharehbaghi, K., Tauchi, T., Burgess, G. S., Miyazawa, K., Jayaram, H. N. & Boswell, H. S. (1993) *Blood* **82,** 1838–1847.
14. Kharbanda, S. M., Sherman, M. L. & Kufe, D. W. (1990) *Blood* **75,** 583–588.
15. Parandoosh, Z., Robins, R. K., Belei, M. & Rubalcava, B. (1989) *Biochem. Biophys. Res. Commun.* **164,** 869–874.
16. Parandoosh, Z., Rubalcava, B., Matsumoto, S. S., Jolley, W. B. & Robins, R. K. (1990) *Life Sci.* **46,** 315–320.
17. Vitale, M., Zamai, L., Falcieri, E., Zauli, G., Gobbi, P., Santi, S., Cinti, C. & Weber, G. (1997) *Cytometry* **30,** 61–66.
18. Olah, E., Csokay, B., Prajda, N., Kote-Jarai, Z., Yeh, Y. A. & Weber, G. (1996) *Anticancer Res.* **16,** 2469–2477.
19. Pall, M. L. (1985) in *Curr. Top. Cell. Regul.*, eds. Horecker, B. L. & Stadtman, E. R. (Academic, New York), Vol. 25, pp. 1–20.
20. Cooney, D. A., Jayaram, H. N., Glazer, R. I., Kelley, J. A., Marquez, V. E., Gebeyehu, G., Van Cott, A. C., Zwelling, L. A. & Johns, D. G. (1983) *Adv. Enzyme Regul.* **21,** 271–303.
21. Tovari, J., Bocsi, J., Ladanyi, A., Lapis, K. & Timar, J. (1996) *Anticancer Res.* **16,** 3307–3312.
22. Lapis, K. Y., Bocsi, J., Tovari, J., Bartha, I., Timar, J. & Raso, E. (1996) *Anticancer Res.* **16,** 3323–3331.
23. Timar, J., Tovari, J., Pogany, G., Ladanyi, A., Paku, S., Rso, E., Bocsi, J., Jeney, A. & Lapis, K. (1996) *Eur. J. Cancer* **32A,** 152–159.
24. Carney, D. N., Ahluwalia, G. S., Jayaram, H. N., Cooney, D. A. & Johns, D. G. (1985) *J. Clin. Invest.* **75,** 175–182.
25. Wright, D. G., Boosalis, M. S., Waraska, K., Oshry, L. J., Weintraub, L. R. & Vosburgh, E. (1996) *Anticancer Res.* **16,** 3349–3351.
26. Tricot, G. & Weber, G. (1996) *Anticancer Res.* **16,** 3341–3347.
27. Weber, G., Nagai, M., Natsumeda, Y., Eble, J. N., Jayaram, H. N., Paulik, E., Zhen, W. N., Hoffman, R. & Tricot, G. (1991) *Cancer Commun.* **3,** 61–66.
28. Alison, A. C., Hovi, T., Watts, R. W. E. & Webster, A. D. B. (1977) *CIBA Found. Symp.* **48,** 207–224.
29. Behrend, M. (1996) *Clin. Nephrol.* **45,** 336–341.
30. Shaw, L. M., Sollinger, H. W., Halloran, P., Morris, R. E., Yatscoff, R. W., Ransom, J., Tsina, I., Keown, P., Holt, D. W., Lieberman, R., *et al.* (1995) *Ther. Drug Monit.* **17,** 690–699.
31. Carr, S. F., Papp, E., Wu, J. C. & Natsumeda, Y. (1993) *J. Biol. Chem.* **268,** 27286–27290.
32. Sintchak, M. D., Fleming, M. A., Futer, O., Raybuck, S. A., Chambers, S. P., Caron, P. R., Murcko, M. A. & Wilson, K. P. (1996) *Cell* **85,** 921–930.
33. Tricot, G., Jayaram, H. N., Weber, G. & Hoffman, R. (1990) *Int. J. Cell Cloning* **8,** 161–170.
34. Knudtzon, S. & Nissen, N. I. (1972) *Cancer Chemother. Rep. - Part 1* **56,** 221–227.
35. Brewin, T. B., Cole, M. P., Jones, C. T., Platt, D. S. & Todd, I. D. (1972) *Cancer Chemother. Rep. - Part 1* **56,** 83–87.
36. Franklin, T. J., Jacobs, V., Bruneau, P. & Ple, P. (1995) *Adv. Enzyme Regul.* **35,** 91–100.
37. Franklin, T. J., Jacobs, V., Jones, G., Ple, P. & Bruneau, P. (1996) *Cancer Res.* **56,** 984–987.
38. Natsumeda, Y., Ohno, S., Kawasaki, H., Konno, Y., Weber, G. & Suzuki, K. (1990) *J. Biol. Chem.* **265,** 5292–5295.
39. Konno, Y., Natsumeda, Y., Nagai, M., Yamaji, Y., Ohno, S., Suzuki, K. & Weber, G. (1991) *J. Biol. Chem.* **266,** 506–509.
40. Senda, M. & Natsumeda, Y. (1994) *Life Sci.* **54,** 1917–1926.
41. Nagai, M., Natsumeda, Y., Konno, Y., Hoffman, R., Irino, S. & Weber, G. (1991) *Cancer Res.* **51,** 3886–3890.
42. Nagai, M., Natsumeda, Y. & Weber, G. (1992) *Cancer Res.* **52,** 258–261.
43. Dayton, J. S., Lindsten, T., Thompson, C. B. & Mitchell, B. S. (1994) *J. Immunol.* **152,** 984–991.
44. Whitby, F. G., Luecke, H., Kuhn, P., Somoza, J. R., Huete-Perez, J. A., Phillips, J. D., Hill, C. P., Fletterick, R. J. & Wang, C. C. (1997) *Biochemistry* **36,** 10666–10674.
45. Gebeyehu, G., Marquez, V. E., Van Cott, A., Cooney, D. A., Kelley, J. A., Jayaram, H. N., Ahluwalia, G. S., Dion, R. L., Wilson, Y. A. & Johns, D. G. (1985) *J. Med. Chem.* **28,** 99–105.
46. Boritzki, T. J., Berry, D. A., Besserer, J. A., Cook, P. D., Fry, D. W., Leopold, W. R. & Jackson, R. C. (1985) *Biochem. Pharmacol.* **34,** 1109–1114.
47. Xiang, B., Taylor, J. C. & Markham, G. D. (1996) *J. Biol. Chem.* **271,** 1435–1440.
48. Rodgers, D. W. (1997) *Methods Enzymol.* **276,** 183–203.
49. Otwinowski, Z. & Minor, W. (1997) *Methods Enzymol.* **276,** 307–326.
50. Drenth, J. (1994) *Principles of Protein X-Ray Crystallography* (Springer, New York).
51. Brünger, A. T. (1990) *Acta Crystallogr. A* **46,** 46–57.
52. Brünger, A. T., Adams, P. D., Clore, G. M., DeLano, W. L., Gros, P., Grosse-Kunstleve, R. W., Jiang, J. S., Kuszewski, J., Nilges, M., Pannu, N. S., *et al.* (1998) *Acta Crystallogr. D* **54,** 905–921.
53. Pannu, N. S. & Read, R. J. (1996) *Acta Crystallogr. A* **52,** 659–668.
54. Read, R. J. (1986) *Acta Crystallogr. A* **42,** 140–149.
55. Cowtan, K. (1994) *Joint CCP4 and ESF-EACBM Newsletter* **31,** 34–38.
56. Hodel, A., Kim, S. H. & Brünger, A. T. (1992) *Acta Crystallogr. A* **48,** 851–858.
57. Corpet, F., Gouzy, J. & Kahn, D. (1998) *Nucleic Acids Res.* **26,** 323–326.
58. Kruger, W. D. & Cox, D. R. (1994) *Proc. Natl. Acad. Sci. USA* **91,** 6614–6618.
59. Srivastava, P. C., Revankar, G. R. & Robins, R. K. (1984) *J. Med. Chem.* **27,** 266–269.
60. Burling, F. T. & Goldstein, B. M. (1992) *J. Am. Chem. Soc.* **114,** 2313–2320.
61. Li, H., Hallows, W. H., Punzi, J. S., Marquez, V. E., Carrell, H. L., Pankiewicz, K. W., Watanabe, K. A. & Goldstein, B. M. (1994) *Biochemistry* **33,** 23–32.
62. Li, M., Dyda, F., Benhar, I., Pastan, I. & Davies, D. (1996) *Proc. Natl. Acad. Sci. USA* **93,** 6902–6906.
63. Link, J. O. & Straub, K. (1996) *J. Am. Chem. Soc.* **118,** 2091–2092.
64. Huete-Perez, J. A., Wu, J. C., Whitby, F. G. & Wang, C. C. (1995) *Biochemistry* **34,** 13889–13894.
65. Schalk-Hihi, C., Zhang, Y.-Z. & Markham, G. D. (1998) *Biochemistry* **37,** 7608–7616.
66. Nimmesgern, E., Fox, T., Fleming, M. A. & Thomson, J. A. (1996) *J. Biol. Chem.* **271,** 19421–19427.
67. Lesiak, K., Watanabe, K. A., Majumdar, A., Powell, J., Seidman, M., Vanderveen, K., Goldstein, B. M. & Pankiewicz, K. W. (1998) *J. Med. Chem.* **41,** 618–622.